Multiqubit controlled unitary gate by adiabatic passage with an optical cavity

Hayato Goto and Kouichi Ichimura
Advanced Materials and Devices Laboratory, Corporate Research and Development Center, Toshiba Corporation, 1 Komukai Toshiba-cho, Saiwai-ku, Kawasaki 212-8582, Japan
(Received 31 October 2003; revised manuscript received 3 February 2004; published 9 July 2004)

A new implementation of quantum gates by adiabatic passage with an optical cavity is proposed. This implementation allows one to perform not only elementary gates, such as one-qubit gates and a controlled-NOT gate, but also multiqubit controlled unitary gates. Some quantum gates are numerically simulated. From the simulation results, it is concluded that this implementation of the three-qubit controlled gates is more efficient than decomposing into the elementary gates.

DOI: 10.1103/PhysRevA.70.012305 PACS number(s): 03.67.Lx, 42.50.−p

I. INTRODUCTION

It is well known that any gate operation in quantum computation can be performed only with one-qubit unitary gates and two-qubit conditional gates, such as controlled-NOT gates [1,2]. In this sense, a set of these elementary gates is universal for quantum computation. Many physical implementations of two-qubit conditional gates have been proposed and demonstrated [3,4]. However, it is desirable that multiqubit gates, such as $(n+1)$-qubit controlled unitary gates with n control qubits $(n=2,3,\cdots)$, are directly and efficiently implemented without decomposing into the elementary gates because the realization of quantum algorithms, such as Shor's algorithm for prime factoring [5] or Grover's algorithm for database search [6], requires many multiqubit gates and because the decomposition of the multiqubit gates into the elementary gates requires a number of gate steps and additional qubits [2,3,7]. Several proposals of efficient implementations of multiqubit gates have been reported [8–14]. These schemes use cold trapped ions coupled to one another through the collective quantized motion [8,9], nuclear magnetic resonance [10,11], cavity photons coupled to one another through atomic beams [12], quantum dots [13], or Cooper pairs in superconducting circuit [14].

In this paper, we propose an implementation of multiqubit controlled unitary gates. This implementation uses ground states of atoms as qubits and utilizes adiabatic passage with a single-mode optical cavity. Adiabatic passage has been used for coherent population transfer [15]. It is advantageous in quantum computation because decoherence due to spontaneous emission from excited states can be avoided and because it is robust against experimental parameter errors. Pellizzari *et al.* have proposed a scheme implementing controlled unitary gates by a combination of Raman transition and adiabatic passage with an optical cavity [16]. Kis and Renzoni have also proposed a method to implement all one-qubit gates via only adiabatic passage [17]. Recently, some proposals for quantum computing via adiabatic passage have been reported, especially in terms of geometric quantum computation [18–20]. The implementation presented in this paper allows adiabatic-passage-only gate operations.

This paper is organized as follows. In Sec. II, the scheme proposed here is explained. In Secs. III–V, we show how to implement one-qubit unitary gates, two-qubit controlled unitary gates, and multiqubit controlled unitary gates in this scheme. In Sec. VI, a one-qubit $\pi/2$ gate, a two-qubit controlled π gate, and a three-qubit controlled π gate are numerically simulated. Furthermore, the efficiency of the implementation of the multiqubit gates is also discussed in Sec. VI. The conclusion is presented in Sec. VII.

II. THE SCHEME

The scheme proposed in this paper is shown in Fig. 1. It is composed of five-level atoms fixed inside a single-mode optical cavity. The three lower levels are assumed to be so stable that the decoherence of them is negligible compared to the decoherence of the two upper levels and the cavity decay. The kth qubit is stored in two of the three lower states, $|0\rangle_k$ and $|1\rangle_k$, in the kth atom. Similar schemes have been proposed before [16,21–24]. The qubits are addressed by their transition frequencies or positions. Two levels of each atom, $|2\rangle_k$ and $|3\rangle_k$, are strongly coupled via the cavity-mode field. This scheme will be realized with trapped ions [16,22–24] or with impurity levels in a solid, such as Pr^{3+} ions in Y_2SiO_5 crystal [25], or nitrogen-vacancy color center in diamond [26]. In the solid-state scheme, it is easy to satisfy a condition that the coupling rates between the five-level atoms and the cavity are constant, while it is relatively difficult in the ion-trap case to satisfy the condition because of fluctuation of the trapped-ion positions.

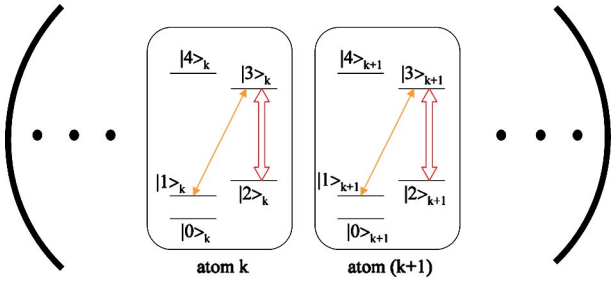

FIG. 1. (Color online) The scheme proposed in this paper. Five-level atoms are fixed inside a single-mode optical cavity. The kth qubit is stored in two of the three lower states, $|0\rangle_k$ and $|1\rangle_k$, in the kth atom. Two levels of each atom, $|2\rangle_k$ and $|3\rangle_k$, are strongly coupled via the cavity-mode field.

In the following sections, we show how to implement quantum gates in this scheme.

III. ONE-QUBIT GATE

In the scheme, one-qubit gates on the kth qubit are performed via adiabatic passage by Kis's method [17] using four of the five states: $|0\rangle_k$, $|1\rangle_k$, $|2\rangle_k$, and $|4\rangle_k$. In the following, we explain the method in detail because the basic idea of the method is applied to multiqubit controlled unitary gates in Secs. IV and V. We also explain the concept of adiabatic passage here. Since the cavity-mode field is not used and is always in the vacuum state during the one-qubit gate operation, the state of the field is omitted in this section. The subscript k is also omitted.

A. One-qubit phase gate

We first show how to implement one-qubit phase gates in the scheme. Next, the one-qubit phase gates will be generalized to one-qubit unitary gates. The operation of the one-qubit phase gate of a phase ϕ is expressed using the initial state $|\psi_0\rangle=\alpha_0|0\rangle+\alpha_1|1\rangle$ as follows:

$$|\psi_0\rangle \rightarrow |\psi\rangle = \alpha_0|0\rangle + e^{i\phi}\alpha_1|1\rangle. \tag{1}$$

Laser pulses resonant with $|1\rangle$-$|4\rangle$ and $|2\rangle$-$|4\rangle$ transitions are used to perform this phase gate. The interaction Hamiltonian in the interaction picture and in the rotating-wave approximation is given by

$$H(t) = \hbar\Omega_1(t)|4\rangle\langle 1| + \hbar\Omega_2(t)|4\rangle\langle 2| + \text{H.c.} \tag{2}$$

Here $\Omega_1(t)$ and $\Omega_2(t)$ are the Rabi frequencies corresponding to the $|1\rangle$-$|4\rangle$ and $|2\rangle$-$|4\rangle$ transitions, respectively, and H.c. denotes the Hermitian conjugate. The terms describing the coupling between the five-level atoms and the cavity-mode field have been removed for simplicity because they have no relation to the time evolution of the state in this process. Moreover, the terms corresponding to decoherence and decay of both the five-level atoms and the cavity have been ignored assuming that the gate operation is finished before the atom decoheres. This Hamiltonian has the following dark state, which is the eigenstate of the Hamiltonian corresponding to zero eigenvalue and is decoupling from the upper states [27]:

$$|D(t)\rangle \propto \Omega_2(t)|1\rangle - \Omega_1(t)|2\rangle, \tag{3}$$

where the proportionality constant is chosen so that $|D(t)\rangle$ is normalized and is initially equal to $|1\rangle$. Under a certain condition, which is called adiabatic condition, the time evolution of the state is given by

$$|\psi(0)\rangle = |\psi_0\rangle \rightarrow |\psi(t)\rangle = \alpha_0|0\rangle + \alpha_1 e^{i\gamma(t)}|D(t)\rangle. \tag{4}$$

This process is called adiabatic passage. Here, the phase $\gamma(t)$, which is given by

$$\gamma(t) = i\int_0^t dt'\langle D(t')|\frac{d}{dt'}|D(t')\rangle, \tag{5}$$

is called Berry phase [28]. This has a geometrical meaning [29] and quantum computations using this geometrical phase have recently been proposed [18–20]. In this paper, however, we consider only the case $\gamma(t)=0$. In this sense, our implementation is different from the geometric quantum computation. $\gamma(t)$ is equal to zero if the phase of $\Omega_j(t)$ changes only when $\Omega_j(t)=0$ $(j=1,2)$. Then, the time evolution of the state is expressed as

$$|\psi(0)\rangle = |\psi_0\rangle \rightarrow |\psi(t)\rangle = \alpha_0|0\rangle + \alpha_1|D(t)\rangle. \tag{6}$$

To perform the phase gate, $|1\rangle$ is first transferred to $|2\rangle$ by this adiabatic passage. Next, $|2\rangle$ is adiabatically transferred back to $e^{i\phi}|1\rangle$. The phase shift ϕ is realized by the phase shift of $\Omega_2(t)$. Thus, it turns out that the phase gate described by Eq. (1) can be achieved via the above adiabatic passage controlling $\Omega_1(t)$ and $\Omega_2(t)$.

An example of the phase gate is shown in Fig. 2 and is explained in Sec. VI.

B. Generalization to one-qubit unitary gate

Here we generalize the one-qubit phase gates to one-qubit unitary gates.

An arbitrary unitary operator U on the Hilbert space spanned by $\{|0\rangle,|1\rangle\}$ can be represented as

$$U = e^{i\theta}(|d\rangle\langle d| + e^{i\phi}|c\rangle\langle c|), \tag{7}$$

with

$$|c\rangle = \cos\frac{\Theta}{2}|0\rangle + e^{i\Phi}\sin\frac{\Theta}{2}|1\rangle, \tag{8}$$

$$|d\rangle = \sin\frac{\Theta}{2}|0\rangle - e^{i\Phi}\cos\frac{\Theta}{2}|1\rangle. \tag{9}$$

Equation (7) means that U has eigenstates $|d\rangle$ and $|c\rangle$ corresponding to eigenvalues $e^{i\theta}$ and $e^{i(\theta+\phi)}$, respectively. The operation of the one-qubit unitary gate that operates U on a qubit $|\psi_0\rangle=\alpha_0|0\rangle+\alpha_1|1\rangle=\alpha_d|d\rangle+\alpha_c|c\rangle$ is expressed as follows:

$$|\psi_0\rangle \rightarrow |\psi\rangle = U|\psi_0\rangle = e^{i\theta}(\alpha_d|d\rangle + e^{i\phi}\alpha_c|c\rangle). \tag{10}$$

To perform the unitary gate, laser pulses resonant with the $|0\rangle$-$|4\rangle$ transition are used in addition to the pulses resonant with $|1\rangle$-$|4\rangle$ and $|2\rangle$-$|4\rangle$ transitions. The Hamiltonian is given by

$$H(t) = \hbar\Omega_0(t)|4\rangle\langle 0| + \hbar\Omega_1(t)|4\rangle\langle 1| + \hbar\Omega_2(t)|4\rangle\langle 2| + \text{H.c.}, \tag{11}$$

where $\Omega_0(t)$, $\Omega_1(t)$, and $\Omega_2(t)$ are the Rabi frequencies corresponding to the $|0\rangle$-$|4\rangle$, $|1\rangle$-$|4\rangle$, and $|2\rangle$-$|4\rangle$ transitions, respectively. $\Omega_0(t)$ and $\Omega_1(t)$ are set as $\Omega_0(t)=\Omega_c(t)\cos\frac{\Theta}{2}$ and $\Omega_1(t)=\Omega_c(t)e^{-i\Phi}\sin\frac{\Theta}{2}$, respectively, with a function $\Omega_c(t)$. The Hamiltonian is then expressed as

$$H(t) = \hbar\Omega_c(t)|4\rangle\langle c| + \hbar\Omega_2(t)|4\rangle\langle 2| + \text{H.c.} \tag{12}$$

$|d\rangle$ is a dark state of the Hamiltonian. From the comparison of Eqs. (2) and (12), it is easily verified that the following operation can be achieved by controlling the Rabi frequencies in a similar manner to the phase gate:

$$|\psi_0\rangle \rightarrow |\psi'\rangle = \alpha_d|d\rangle + e^{i\phi}\alpha_c|c\rangle = e^{-i\theta}U|\psi_0\rangle. \quad (13)$$

This operation is equivalent to that of the unitary gate described by Eq. (10) except for the global phase θ. The global phase is not important in quantum computation. Thus, it is shown that the one-qubit unitary gates can be performed via adiabatic passage in the present scheme.

IV. CONTROLLED UNITARY GATE

In this section, we show how to implement controlled unitary gates in our scheme. First, controlled phase gates are explained. Next, the controlled phase gates are generalized to controlled unitary gates in a similar manner to the generalization of the one-qubit phase gates to the one-qubit unitary gates.

A. Controlled phase gate

The initial state $|\psi_0\rangle$ is defined as

$$|\psi_0\rangle = \sum_{l_1,l_2=0,1} \alpha_{l_1,l_2}|l_1 l_2\rangle|0\rangle, \quad (14)$$

where $|l_1 l_2\rangle = |l_1\rangle_1|l_2\rangle_2$ and α_{l_1,l_2} denote a state of the two five-level atoms and the probability amplitude of $|l_1 l_2\rangle$ $(l_1, l_2 = 0, 1)$, respectively, and $|0\rangle$ denotes the vacuum state of the cavity-mode field. The output state of the controlled phase gate is defined as

$$|\psi\rangle = \sum_{l_1,l_2=0,1} e^{il_1 l_2\phi}\alpha_{l_1,l_2}|l_1 l_2\rangle|0\rangle. \quad (15)$$

The procedure for the controlled phase gate is composed of the following three steps.

(Step 1) $|1\rangle_2$ is transferred to $|2\rangle_2$ by adiabatic passage with laser pulses resonant with $|1\rangle_2$-$|4\rangle_2$ and $|2\rangle_2$-$|4\rangle_2$ transitions. The state then becomes

$$|\psi_1\rangle = \sum_{l_1=0,1} (\alpha_{l_1,0}|l_1 0\rangle + \alpha_{l_1,1}|l_1 2\rangle)|0\rangle. \quad (16)$$

(Step 2) The phase of $|02\rangle|0\rangle$ is shifted by adiabatic passage with laser pulses resonant with $|0\rangle_1$-$|3\rangle_1$ and $|1\rangle_2$-$|3\rangle_2$ transitions in order to obtain the following state:

$$|\psi_2\rangle = \sum_{l_1=0,1} [\alpha_{l_1,0}|l_1 0\rangle + e^{i(l_1-1)\phi}\alpha_{l_1,1}|l_1 2\rangle]|0\rangle. \quad (17)$$

The detail of this step is explained later.

(Step 3) $|2\rangle_2$ is adiabatically transferred back to $e^{i\phi}|1\rangle_2$ as in Step 1. As a result, we obtain

$$|\psi_3\rangle = \sum_{l_1,l_2=0,1} e^{il_1 l_2\phi}\alpha_{l_1,l_2}|l_1 l_2\rangle|0\rangle. \quad (18)$$

The final state is the same as the output of the controlled phase gate. Thus, it turns out that the controlled phase gate can be performed by the above three steps.

In the following, we explain the detail of Step 2. The Hamiltonian in Step 2 is given by

$$H(t) = \hbar\Omega^{(1)}(t)|3\rangle_{11}\langle 0| + \hbar\Omega^{(2)}(t)|3\rangle_{22}\langle 1| + \sum_{k=1,2} \hbar g^{(k)} a|3\rangle_{kk}\langle 2| + \text{H.c.} \quad (19)$$

Here $\Omega^{(1)}(t)$ and $\Omega^{(2)}(t)$ are the Rabi frequencies corresponding to the $|0\rangle_1$-$|3\rangle_1$ and $|1\rangle_2$-$|3\rangle_2$ transitions, respectively, $g^{(k)}$ is a coupling rate between the kth atom and the cavity-mode field $(k=1,2)$, which is dependent on the position of the kth atom [30], and a is the annihilation operator for cavity photons. This Hamiltonian has the following dark states:

$$|D_{00}\rangle \propto g^{(1)}|00\rangle|0\rangle - \Omega^{(1)}|20\rangle|1\rangle,$$

$$|D_{02}\rangle \propto g^{(1)}\Omega^{(2)}|02\rangle|0\rangle + g^{(2)}\Omega^{(1)}|21\rangle|0\rangle - \Omega^{(1)}\Omega^{(2)}|22\rangle|1\rangle, \quad (20)$$

where the proportionality constants are chosen so that $|D_{00}(t)\rangle$ and $|D_{02}(t)\rangle$ are normalized and are initially equal to $|00\rangle|0\rangle$ and $|02\rangle|0\rangle$, respectively. Under the adiabatic condition and the condition that the Berry phase is equal to zero, the evolution of the state in Step 2 is described as follows:

$$|\psi_1\rangle \rightarrow |\psi(t)\rangle = \alpha_{0,0}|D_{00}(t)\rangle + \alpha_{0,1}|D_{02}(t)\rangle + \alpha_{1,0}|10\rangle|0\rangle + \alpha_{1,1}|12\rangle|0\rangle. \quad (21)$$

The desired phase shift of $|02\rangle|0\rangle$ can be achieved by the phase shift of $\Omega^{(2)}(t)$.

An example of the controlled phase gate is shown in Fig. 3 and is explained in Sec. VI.

B. Generalization to controlled unitary gate

As in the case of the one-qubit unitary gate, the above controlled phase gate can be generalized to controlled unitary gates.

The unitary operator which is operated on the second qubit depending on the state of the first qubit is represented as Eq. (7) with Eqs. (8) and (9). The initial state is represented using $|c\rangle_2$ and $|d\rangle_2$ as follows:

$$|\psi_0\rangle = \sum_{l_1,l_2=0,1} \alpha_{l_1,l_2}|l_1 l_2\rangle|0\rangle = \sum_{\substack{l_1=0,1 \\ l_2'=c,d}} \alpha_{l_1,l_2'}|l_1 l_2'\rangle|0\rangle. \quad (22)$$

In a similar manner to the case of the one-qubit unitary gate, we can obtain the following states instead of the states given by Eqs. (16)–(18):

$$|\psi_1'\rangle = \sum_{l_1=0,1} (\alpha_{l_1,d}|l_1 d\rangle + \alpha_{l_1,c}|l_1 2\rangle)|0\rangle, \quad (23)$$

$$|\psi_2'\rangle = \sum_{l_1=0,1} [\alpha_{l_1,d}|l_1 d\rangle + e^{i(l_1-1)\phi}\alpha_{l_1,c}|l_1 2\rangle]|0\rangle, \quad (24)$$

$$|\psi_3'\rangle = \sum_{l_1=0,1} (\alpha_{l_1,d}|l_1 d\rangle + e^{il_1\phi}\alpha_{l_1,c}|l_1 c\rangle)|0\rangle. \quad (25)$$

The final state can be expressed with U as follows:

$$
\begin{aligned}
|\psi_3'\rangle &= |0\rangle_1(\alpha_{0,d}|d\rangle_2 + \alpha_{0,c}|c\rangle_2)|0\rangle + |1\rangle_1(\alpha_{1,d}|d\rangle_2 \\
&\quad + e^{i\phi}\alpha_{1,c}|c\rangle_2)|0\rangle \\
&= |0\rangle_1(\alpha_{0,d}|d\rangle_2 + \alpha_{0,c}|c\rangle_2)|0\rangle + e^{-i\theta}|1\rangle_1 U(\alpha_{1,d}|d\rangle_2 \\
&\quad + \alpha_{1,c}|c\rangle_2)|0\rangle \\
&= |0\rangle_1(\alpha_{0,0}|0\rangle_2 + \alpha_{0,1}|1\rangle_2)|0\rangle \\
&\quad + e^{-i\theta}|1\rangle_1 U(\alpha_{1,0}|0\rangle_2 + \alpha_{1,1}|1\rangle_2)|0\rangle. \qquad (26)
\end{aligned}
$$

This is equal to the output of the controlled unitary gate except for the phase factor $e^{-i\theta}$. The additional phase factor can be eliminated by a one-qubit phase gate on the first qubit. In the case of a controlled-NOT (CNOT) gate, however, $|\psi_3'\rangle$ is exactly equal to the output of the CNOT gate because the eigenvalues of U corresponding to the CNOT gate are ± 1 and θ can be set to zero. Therefore, the additional phase gate is not necessary to perform the CNOT gate.

V. MULTIQUBIT CONTROLLED UNITARY GATE

In Secs. III and IV, we have shown how to implement one-qubit unitary gates and two-qubit controlled unitary gates by adiabatic passage in our scheme. Since the set of these elementary gates is universal for quantum computation, any quantum gate can be decomposed into them. For example, a three-qubit controlled unitary gate with two control qubits and a unitary operator U on a target qubit, which is denoted by a C^2-U gate, can be decomposed into two CNOT gates, two C-V gates ($V^2=U$), and a C-$V^\dagger$ gate [2]. A C^n-U gate ($n=3,4,\cdots$) can be decomposed into $2(n-1)$ Toffoli gates (C^2-NOT gates) and a C-U gate with $(n-1)$ additional work qubits [3]. However, it is desirable to implement the multiqubit gates more efficiently than decomposing into the elementary gates because the decomposition into the elementary gates requires many gate steps and additional qubits which will induce some problems such as a long gate time or decoherence.

In this section, it is shown that multiqubit controlled phase gates can be performed by adiabatic passage in the present scheme without decomposing into the elementary gates. The efficiency of the multiqubit gates is discussed in Sec. VI. Here we show only how to implement the multiqubit controlled phase gates because multiqubit controlled unitary gates can be realized in a similar manner to the multiqubit controlled phase gates as in the case of the two-qubit controlled unitary gates explained in the last section.

A. Three-qubit controlled phase gate

Before explaining general multiqubit controlled phase gates, we explain the case of a three-qubit controlled phase gate with two control qubits. The initial state $|\psi_0\rangle$ is defined as

$$
|\psi_0\rangle = \sum_{l_1,l_2,l_3=0,1} \alpha_{l_1,l_2,l_3}|l_1 l_2 l_3\rangle|0\rangle, \qquad (27)
$$

where $|l_1 l_2 l_3\rangle = |l_1\rangle_1|l_2\rangle_2|l_3\rangle_3$ and α_{l_1,l_2,l_3} denote a state of the three five-level atoms and the probability amplitude of $|l_1 l_2 l_3\rangle$ $(l_1,l_2,l_3=0,1)$, respectively, and $|0\rangle$ denotes the vacuum state of the cavity-mode field. The output state of the three-qubit controlled phase gate is defined as

$$
|\psi\rangle = \sum_{l_1,l_2,l_3=0,1} e^{il_1 l_2 l_3\phi}\alpha_{l_1,l_2,l_3}|l_1 l_2 l_3\rangle|0\rangle. \qquad (28)
$$

The procedure for this gate is composed of the following three steps as in the case of the two-qubit controlled phase gate.

(Step 1) $|1\rangle_3$ is adiabatically transferred to $|2\rangle_3$ with laser pulses resonant with $|1\rangle_3$-$|4\rangle_3$ and $|2\rangle_3$-$|4\rangle_3$ transitions. The state then becomes

$$
|\psi_1\rangle = \sum_{l_1,l_2=0,1} (\alpha_{l_1,l_2,0}|l_1 l_2 0\rangle + \alpha_{l_1,l_2,1}|l_1 l_2 2\rangle)|0\rangle. \qquad (29)
$$

(Step 2) The phases of $|012\rangle|0\rangle$, $|102\rangle|0\rangle$, and $|002\rangle|0\rangle$ are shifted by adiabatic passage with laser pulses resonant with $|0\rangle_1$-$|3\rangle_1$, $|0\rangle_2$-$|3\rangle_2$, and $|1\rangle_3$-$|3\rangle_3$ transitions in order to obtain the following state:

$$
|\psi_2\rangle = \sum_{l_1,l_2=0,1} [\alpha_{l_1,l_2,0}|l_1 l_2 0\rangle + e^{i(l_1 l_2 - 1)\phi}\alpha_{l_1,l_2,1}|l_1 l_2 2\rangle]|0\rangle. \qquad (30)
$$

The detail of this step is explained later.

(Step 3) $|2\rangle_3$ is adiabatically transferred back to $e^{i\phi}|1\rangle_3$ as in Step 1. As a result, we obtain

$$
|\psi_3\rangle = \sum_{l_1,l_2,l_3=0,1} e^{il_1 l_2 l_3\phi}\alpha_{l_1,l_2,l_3}|l_1 l_2 l_3\rangle|0\rangle. \qquad (31)
$$

The final state is the same as the output of the three-qubit controlled phase gate.

In the following, we explain the detail of Step 2. The Hamiltonian in Step 2 is given by

$$
\begin{aligned}
H(t) &= \hbar\Omega^{(1)}(t)|3\rangle_{11}\langle 0| + \hbar\Omega^{(2)}(t)|3\rangle_{22}\langle 0| + \hbar\Omega^{(3)}(t)|3\rangle_{33}\langle 1| \\
&\quad + \sum_{k=1,2,3} \hbar g^{(k)} a|3\rangle_{kk}\langle 2| + \text{H.c.} \qquad (32)
\end{aligned}
$$

Here $\Omega^{(1)}(t)$, $\Omega^{(2)}(t)$, and $\Omega^{(3)}(t)$ are the Rabi frequencies corresponding to the $|0\rangle_1$-$|3\rangle_1$, $|0\rangle_2$-$|3\rangle_2$, and $|1\rangle_3$-$|3\rangle_3$ transitions, respectively, and $g^{(k)}$ is a coupling rate between the kth atom and the cavity-mode field $(k=1,2,3)$. This Hamiltonian has the following dark states:

$$
\begin{aligned}
|D_{000}\rangle &\propto \sqrt{2}g^{(1)}g^{(2)}|000\rangle|0\rangle - \sqrt{2}g^{(1)}\Omega^{(2)}|020\rangle|1\rangle \\
&\quad - \sqrt{2}g^{(2)}\Omega^{(1)}|200\rangle|1\rangle + \Omega^{(1)}\Omega^{(2)}|220\rangle|2\rangle,
\end{aligned}
$$

$$
|D_{010}\rangle \propto g^{(1)}|010\rangle|0\rangle - \Omega^{(1)}|210\rangle|1\rangle,
$$

$$
|D_{100}\rangle \propto g^{(2)}|100\rangle|0\rangle - \Omega^{(2)}|120\rangle|1\rangle,
$$

$$
\begin{aligned}
|D_{012}\rangle &\propto g^{(1)}\Omega^{(3)}|012\rangle|0\rangle + g^{(3)}\Omega^{(1)}|211\rangle|0\rangle \\
&\quad - \Omega^{(1)}\Omega^{(3)}|212\rangle|1\rangle,
\end{aligned}
$$

$$
\begin{aligned}
|D_{102}\rangle &\propto g^{(2)}\Omega^{(3)}|102\rangle|0\rangle + g^{(3)}\Omega^{(2)}|121\rangle|0\rangle \\
&\quad - \Omega^{(2)}\Omega^{(3)}|122\rangle|1\rangle,
\end{aligned}
$$

$$|D_{002}\rangle \propto \sqrt{2}g^{(1)}g^{(2)}\Omega^{(3)}|002\rangle|0\rangle + \sqrt{2}g^{(2)}g^{(3)}\Omega^{(1)}|201\rangle|0\rangle + \sqrt{2}g^{(3)}g^{(1)}\Omega^{(2)}|021\rangle|0\rangle - \sqrt{2}g^{(1)}\Omega^{(2)}\Omega^{(3)}|022\rangle|1\rangle - \sqrt{2}g^{(2)}\Omega^{(3)}\Omega^{(1)}|202\rangle|1\rangle - \sqrt{2}g^{(3)}\Omega^{(1)}\Omega^{(2)}|221\rangle|1\rangle + \Omega^{(1)}\Omega^{(2)}\Omega^{(3)}|222\rangle|2\rangle, \quad (33)$$

where the proportionality constants are chosen so that $|D_{l_1 l_2 l_3}(t)\rangle$ is normalized and is initially equal to $|l_1 l_2 l_3\rangle|0\rangle$. The dark states with relation to the evolution of the state are only them when $g^{(1)}=g^{(2)}=g^{(3)}$ and $(|\Omega^{(1)}|-|\Omega^{(2)}|)(|\Omega^{(2)}|-|\Omega^{(3)}|)(|\Omega^{(3)}|-|\Omega^{(1)}|)\neq 0$. Under the adiabatic condition and the condition that the Berry phase is equal to zero, the evolution of the state in Step 2 is given by

$$|\psi_1\rangle \rightarrow |\psi(t)\rangle = \alpha_{0,0,0}|D_{000}(t)\rangle + \alpha_{0,0,1}|D_{002}(t)\rangle + \alpha_{0,1,0}|D_{010}(t)\rangle + \alpha_{0,1,1}|D_{012}(t)\rangle + \alpha_{1,0,0}|D_{100}(t)\rangle + \alpha_{1,0,1}|D_{102}(t)\rangle + \alpha_{1,1,0}|110\rangle|0\rangle + \alpha_{1,1,1}|112\rangle|0\rangle. \quad (34)$$

The desired phase shifts of $|012\rangle|0\rangle$, $|102\rangle|0\rangle$, and $|002\rangle|0\rangle$ can be achieved by the phase shift of $\Omega^{(3)}(t)$.

An example of the three-qubit controlled phase gate is shown in Fig. 4 and is explained in Sec. VI.

B. $(n+1)$-qubit controlled phase gate

In general, $(n+1)$-qubit controlled phase gates with n control qubits $(n=1,2,\cdots)$ can be performed by the following three steps as in the cases of the two-qubit and three-qubit controlled phase gates. The initial state $|\psi_0\rangle$ is defined as

$$|\psi_0\rangle = \sum_{l_1,l_2,\cdots,l_{n+1}=0,1} \alpha_{l_1,l_2,\cdots,l_{n+1}}|l_1 l_2 \cdots l_{n+1}\rangle|0\rangle. \quad (35)$$

(Step 1) $|1\rangle_{n+1}$ is adiabatically transferred to $|2\rangle_{n+1}$. The state then becomes

$$|\psi_1\rangle = \sum_{l_1,\cdots,l_n=0,1} (\alpha_{l_1,\cdots,l_n,0}|l_1\cdots l_n 0\rangle + \alpha_{l_1,\cdots,l_n,1}|l_1\cdots l_n 2\rangle)|0\rangle. \quad (36)$$

(Step 2) The phases of $|l_1\cdots l_n 2\rangle$ $(l_1,\cdots,l_n=0,1$, except for $l_1=l_2=\cdots=l_n=1)$ are shifted by adiabatic passage with laser pulses resonant with $|0\rangle_k$-$|3\rangle_k$ $(k=1,2,\cdots,n)$ and $|1\rangle_{n+1}$-$|3\rangle_{n+1}$ transitions in order to obtain the following state:

$$|\psi_2\rangle = \sum_{l_1,\cdots,l_n=0,1} [\alpha_{l_1,\cdots,l_n,0}|l_1\cdots l_n 0\rangle + e^{i(\prod_{k=1}^{n} l_k - 1)\phi}\alpha_{l_1,\cdots,l_n,1}|l_1\cdots l_n 2\rangle|0\rangle. \quad (37)$$

The detail of this step is explained later.

(Step 3) $|2\rangle_{n+1}$ is adiabatically transferred back to $e^{i\phi}|1\rangle_{n+1}$. As a result, we obtain

$$|\psi_3\rangle = \sum_{l_1,\cdots,l_{n+1}=0,1} e^{i\phi\prod_{k=1}^{n+1} l_k}\alpha_{l_1,\cdots,l_{n+1}}|l_1\cdots l_{n+1}\rangle|0\rangle. \quad (38)$$

Thus, the $(n+1)$-qubit controlled phase gate can be realized by the above three steps.

In the following, we explain the detail of Step 2. The Hamiltonian in Step 2 is given by

$$H(t) = \sum_{k=1}^{n} \hbar\Omega^{(k)}(t)|3\rangle_{kk}\langle 0| + \hbar\Omega^{(n+1)}(t)|3\rangle_{n+1n+1}\langle 1| + \sum_{k=1}^{n+1} \hbar g^{(k)}a|3\rangle_{kk}\langle 2| + \text{H.c.} \quad (39)$$

This Hamiltonian has the following dark states:

$$|D_{01\cdots 10}\rangle \propto \Omega^{(1)} \exp\left[-\frac{g^{(1)}a}{\Omega^{(1)}}|0\rangle_{11}\langle 2|\right]|21\cdots 10\rangle|1\rangle,\cdots,$$

$$|D_{0\cdots 00}\rangle \propto \prod_{k'=1}^{n}\Omega^{(k')} \exp\left[-\sum_{k=1}^{n}\frac{g^{(k)}a}{\Omega^{(k)}}|0\rangle_{kk}\langle 2|\right]|2\cdots 20\rangle|n\rangle,$$

$$|D_{01\cdots 12}\rangle \propto \Omega^{(1)}\Omega^{(n+1)} \exp\left[-\frac{g^{(1)}a}{\Omega^{(1)}}|0\rangle_{11}\langle 2| - \frac{g^{(n+1)}a}{\Omega^{(n+1)}}|1\rangle_{n+1n+1}\langle 2|\right]|21\cdots 12\rangle|1\rangle,\cdots, \quad (40)$$

$$|D_{0\cdots 02}\rangle \propto \prod_{k'=1}^{n}\Omega^{(k')}\Omega^{(n+1)} \exp\left[-\sum_{k=1}^{n}\frac{g^{(k)}a}{\Omega^{(k)}}|0\rangle_{kk}\langle 2| - \frac{g^{(n+1)}a}{\Omega^{(n+1)}}|1\rangle_{n+1n+1}\langle 2|\right]|2\cdots 22\rangle|n\rangle,$$

where the proportionality constants are chosen so that $|D_{l_1\cdots l_{n+1}}(t)\rangle$ is normalized and is initially equal to $|l_1\cdots l_{n+1}\rangle|0\rangle$. The desired phase shifts can be achieved by the phase shift of $\Omega^{(n+1)}(t)$.

VI. NUMERICAL SIMULATIONS

In this section, a one-qubit $\pi/2$ gate, a two-qubit controlled π gate, and a three-qubit π gate are simulated by numerically solving Schrödinger equations. By comparing the simulation results of the two-qubit and three-qubit gates, the efficiency of the present implementation of the multiqubit gates is discussed.

A. One-qubit phase gate

Figure 2 shows the simulation result of a one-qubit $\pi/2$ gate with the following initial state:

$$|\psi(0)\rangle = \frac{|0\rangle + |1\rangle}{\sqrt{2}}. \quad (41)$$

Figure 2(a) shows the absolute values of the Rabi frequencies, $|\Omega_1(t)|$ (solid line) and $|\Omega_2(t)|$ (dashed line). Figure 2(b) shows the phases of the Rabi frequencies, $\arg[\Omega_1(t)]$ (solid line) and $\arg[\Omega_2(t)]$ (dashed line). Figures 2(c) and 2(d) show the real part (solid line) and imaginary part

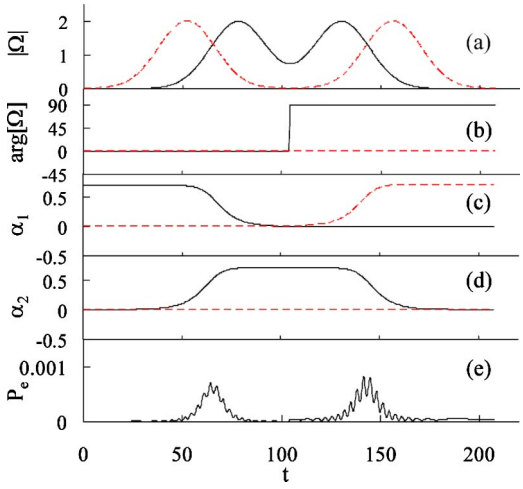

FIG. 2. (Color online) Numerical simulation of a one-qubit $\pi/2$ gate. Time and Rabi frequencies are measured in arbitrary units. (a) Absolute values of the Rabi frequencies. Solid line: $|\Omega_1(t)|$. Dashed line: $|\Omega_2(t)|$. (b) Phases (degree) of the Rabi frequencies. Solid line: $\arg[\Omega_1(t)]$. Dashed line: $\arg[\Omega_2(t)]$. (c) Real part (solid line) and imaginary part (dashed line) of the probability amplitude of $|1\rangle$. (d) Real part (solid line) and imaginary part (dashed line) of the probability amplitude of $|2\rangle$. (e) Error probability $P_e(t)$ defined by Eq. (43).

(dashed line) of the probability amplitudes of $|1\rangle$ and $|2\rangle$, respectively. On the other hand, the amplitude of $|0\rangle$ is constant in this process. As expected, the final state is

$$|\psi\rangle = \frac{|0\rangle + i|1\rangle}{\sqrt{2}}. \tag{42}$$

Therefore, the one-qubit $\pi/2$ gate is realized by this process.

Figure 2(e) shows the error probability defined by the following equation:

$$P_e(t) = 1 - |\langle\psi(t)|\psi_s(t)\rangle|^2. \tag{43}$$

Here $|\psi_s(t)\rangle$ is the state obtained by the simulation and $|\psi(t)\rangle$ is the dark state defined by Eq. (6). $P_e(t)$ is very small during the gate operation. This means that the state is almost always in the dark state and also means that the upper states are almost unpopulated as expected.

B. Controlled phase gate

Figure 3 shows the simulation result of a controlled π gate with the following initial state:

$$|\psi(0)\rangle = \frac{(|00\rangle + |01\rangle + |10\rangle + |11\rangle)|0\rangle}{2}. \tag{44}$$

The coupling rates were chosen as $g^{(1)}=g^{(2)}=g$. Figure 3(a) shows the scaled Rabi frequencies: $\Omega_1(t)/g$ (solid line), $\Omega_2(t)/g$ (dashed line), $\Omega^{(1)}/g$ (dotted line), and $\Omega^{(2)}/g$ (dot-dashed line), where $\Omega_1(t)$ and $\Omega_2(t)$ are the Rabi frequencies of the pulses resonant with $|1\rangle_2-|4\rangle_2$ and $|2\rangle_2-|4\rangle_2$ transitions, respectively, and used in Step 1 and Step 3. Figure 3(b) shows the probability amplitudes of $|00\rangle|0\rangle$ (solid line) and

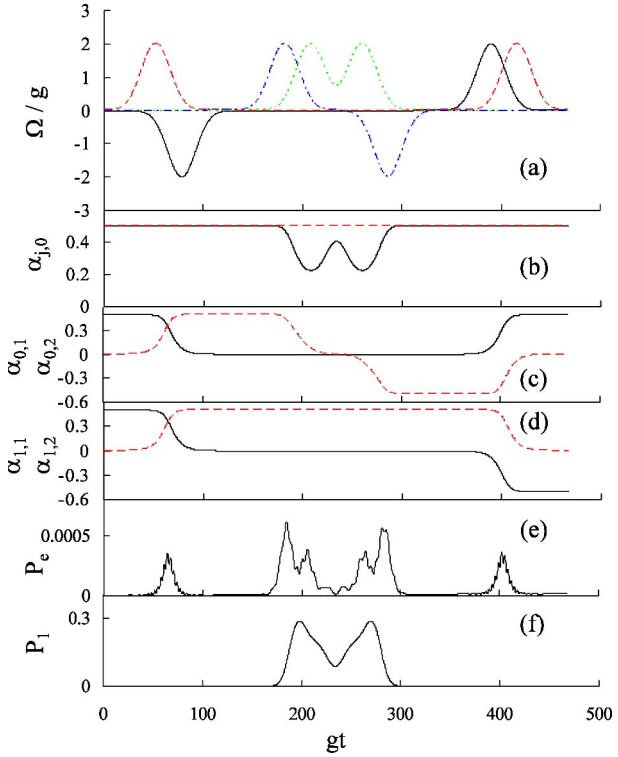

FIG. 3. (Color online) Numerical simulation of a controlled π gate. The coupling rates were chosen as $g^{(1)}=g^{(2)}=g$. (a) Scaled Rabi frequencies. Solid line: $\Omega_1(t)/g$. Dashed line: $\Omega_2(t)/g$. Dotted line: $\Omega^{(1)}(t)/g$. Dot-dashed line: $\Omega^{(2)}(t)/g$. Here $\Omega_1(t)$ and $\Omega_2(t)$ are the Rabi frequencies of the pulses resonant with $|1\rangle_2-|4\rangle_2$ and $|2\rangle_2-|4\rangle_2$ transitions, respectively, and used in Step 1 and Step 3. (b) Probability amplitudes of $|00\rangle|0\rangle$ (solid line) and $|10\rangle|0\rangle$ (dashed line). (c) Probability amplitudes of $|01\rangle|0\rangle$ (solid line) and $|02\rangle|0\rangle$ (dashed line). (d) Probability amplitudes of $|11\rangle|0\rangle$ (solid line) and $|12\rangle|0\rangle$ (dashed line). (e) Error probability $P_e(t)$ defined as in the case of the one-qubit $\pi/2$ gate. (f) Probability that the number of the cavity-mode photons is one, which is denoted by $P_1(t)$.

$|10\rangle|0\rangle$ (dashed line). Figure 3(c) shows the probability amplitudes of $|01\rangle|0\rangle$ (solid line) and $|02\rangle|0\rangle$ (dashed line). Figure 3(d) shows the probability amplitudes of $|11\rangle|0\rangle$ (solid line) and $|12\rangle|0\rangle$ (dashed line). As expected, the final state is

$$|\psi\rangle = \frac{(|00\rangle + |01\rangle + |10\rangle - |11\rangle)|0\rangle}{2}. \tag{45}$$

Therefore, the controlled π gate is realized by this process.

Figure 3(e) shows the error probability defined as in the case of the one-qubit $\pi/2$ gate. $P_e(t)$ is very small during the gate operation. This means that the state is almost always in the dark state and also means that the upper states are almost unpopulated as expected.

Figure 3(f) shows the probability that the number of the cavity-mode photons is one, which is denoted by $P_1(t)$. This is compared with that of the three-qubit π gate later.

C. Three-qubit controlled phase gate

Figure 4 shows the simulation result of a three-qubit controlled π gate with two control qubits. The initial state was defined as

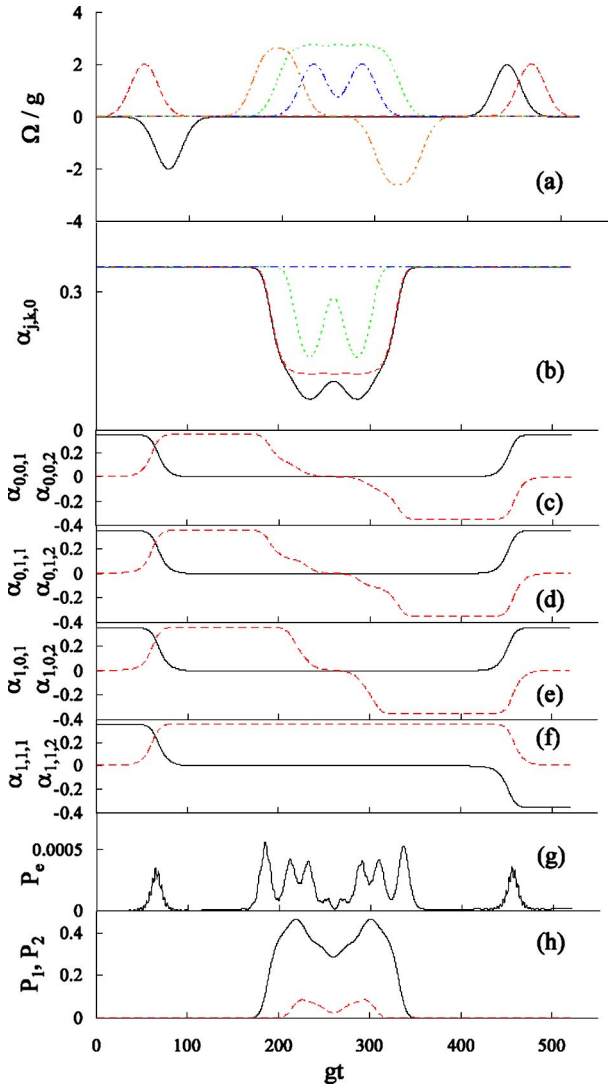

FIG. 4. (Color online) Numerical simulation of a three-qubit controlled π gate with two control qubits. The coupling rates were chosen as $g^{(1)}=g^{(2)}=g^{(3)}=g$. (a) Scaled Rabi frequencies. Solid line: $\Omega_1(t)/g$. Dashed line: $\Omega_2(t)/g$. Dotted line: $\Omega^{(1)}(t)/g$. Dot-dashed line: $\Omega^{(2)}(t)/g$. Dot-dot-dashed line: $\Omega^{(3)}(t)/g$. Here $\Omega_1(t)$ and $\Omega_2(t)$ are the Rabi frequencies of the pulses resonant with $|1\rangle_3-|4\rangle_3$ and $|2\rangle_3-|4\rangle_3$ transitions, respectively, and used in Step 1 and Step 3. (b) Probability amplitudes of $|000\rangle|0\rangle$ (solid line), $|010\rangle|0\rangle$ (dashed line), $|100\rangle|0\rangle$ (dotted line), and $|110\rangle|0\rangle$ (dot-dashed line). (c) Probability amplitudes of $|001\rangle|0\rangle$ (solid line) and $|002\rangle|0\rangle$ (dashed line). (d) Probability amplitudes of $|011\rangle|0\rangle$ (solid line) and $|012\rangle|0\rangle$ (dashed line). (e) Probability amplitudes of $|101\rangle|0\rangle$ (solid line) and $|102\rangle|0\rangle$ (dashed line). (f) Probability amplitudes of $|111\rangle|0\rangle$ (solid line) and $|112\rangle|0\rangle$ (dashed line). (g) Error probability $P_e(t)$ defined as in the case of the one-qubit $\pi/2$ gate. (h) Probability that the number of the cavity-mode photons is equal to j, which is denoted by $P_j(t)$ $(j=1,2)$. Solid line: $P_1(t)$. Dashed line: $P_2(t)$.

$$|\psi(0)\rangle=\frac{1}{2\sqrt{2}}\sum_{l_1,l_2,l_3=0,1}|l_1l_2l_3\rangle|0\rangle. \tag{46}$$

The coupling rates were chosen as $g^{(1)}=g^{(2)}=g^{(3)}=g$. Figure 4(a) shows the scaled Rabi frequencies: $\Omega_1(t)/g$ (solid line), $\Omega_2(t)/g$ (dashed line), $\Omega^{(1)}/g$ (dotted line), $\Omega^{(2)}/g$ (dot-dashed line), and $\Omega^{(3)}/g$ (dot-dot-dashed line), where $\Omega_1(t)$ and $\Omega_2(t)$ are the Rabi frequencies of the pulses resonant with $|1\rangle_3-|4\rangle_3$ and $|2\rangle_3-|4\rangle_3$ transitions, respectively, and used in Step 1 and Step 3. The shapes of $\Omega^{(1)}/g$, $\Omega^{(2)}/g$, and $\Omega^{(3)}/g$ were chosen so that $(|\Omega^{(1)}|-|\Omega^{(2)}|)(|\Omega^{(2)}|-|\Omega^{(3)}|)\times(|\Omega^{(3)}|-|\Omega^{(1)}|)\neq 0$ is satisfied because then the dark states with relation to time evolution are only the states shown by Eq. (33). Figure 4(b) shows the probability amplitudes of $|000\rangle|0\rangle$ (solid line), $|010\rangle|0\rangle$ (dashed line), $|100\rangle|0\rangle$ (dotted line), and $|110\rangle|0\rangle$ (dot-dashed line). Figure 4(c) shows the probability amplitudes of $|001\rangle|0\rangle$ (solid line) and $|002\rangle|0\rangle$ (dashed line). Figure 4(d) shows the probability amplitudes of $|011\rangle|0\rangle$ (solid line) and $|012\rangle|0\rangle$ (dashed line). Figure 4(e) shows the probability amplitudes of $|101\rangle|0\rangle$ (solid line) and $|102\rangle|0\rangle$ (dashed line). Figure 4(f) shows the probability amplitudes of $|111\rangle|0\rangle$ (solid line) and $|112\rangle|0\rangle$ (dashed line). As expected, the final state is

$$|\psi\rangle=\frac{1}{2\sqrt{2}}\sum_{l_1,l_2,l_3=0,1}(-1)^{l_1l_2l_3}|l_1l_2l_3\rangle|0\rangle. \tag{47}$$

Therefore, the three-qubit controlled π gate is realized by this process.

From Figs. 3 and 4, it turns out that the gate time of the three-qubit controlled π gate is nearly equal to that of the two-qubit controlled π gate. On the other hand, the three-qubit controlled π gate can be decomposed into five two-qubit controlled gates (see Fig. 5). Therefore, the present implementation of the three-qubit controlled π gate is about five times as fast as decomposing into two-qubit controlled gates.

Figure 4(g) shows the error probability defined as in the case of the one-qubit $\pi/2$ gate. $P_e(t)$ is very small during the gate operation. This means that the state is almost always in the dark state and also means that the upper states are almost unpopulated as expected. By comparing Figs. 3(e) and 4(g), we also find it is not the case that decoherence due to spontaneous emission from the upper states in the case of the three-qubit controlled gate is much faster than in the case of the two-qubit controlled gate.

Figure 4(h) shows the probability that the number of the cavity-mode photons is equal to j, which is denoted by $P_j(t)$ $(j=1,2)$. By comparing Figs. 3(f) and 4(h), we find it is not the case that decoherence due to cavity decay in the case of the three-qubit controlled gate is much faster than in the case of the two-qubit controlled gate.

From the above comparison of the three-qubit and two-qubit controlled gates, it is concluded that the present implementation of the three-qubit controlled gates is more efficient than decomposing into the elementary gates.

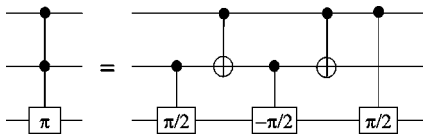

FIG. 5. Decomposition of the three-qubit controlled π gate into two controlled-NOT gates, two controlled $\pi/2$ gates, and a controlled $(-\pi/2)$ gate.

In the following, we discuss the case of $(n+1)$-qubit controlled unitary gates $(n=3,4,\cdots)$. In the case without additional work qubits, $(n+1)$-qubit controlled unitary gates can be decomposed into $(2^{n+1}-3)$ two-qubit controlled gates [2]. In the case with $(n-1)$ additional work qubits, which are undesirable because they will induce additional decoherence, $(n+1)$-qubit controlled unitary gates can be decomposed into $2(n-1)$ Toffoli gates and a two-qubit controlled gate [3]. Since a Toffoli gate is decomposed into five two-qubit controlled gates, $(n+1)$-qubit controlled gates are decomposed into $(10n-9)$ two-qubit controlled gates in the case with work qubits. On the other hand, if $(n+1)$-qubit controlled gates can be realized in our scheme by choosing the pulse shapes of the Rabi frequencies $\Omega^{(k)}(t)$ $(k=1,2,\cdots,n+1)$ so that all $|\Omega^{(k)}(t)|$ are almost always unequal to one another as the case of the three-qubit controlled gates, the gate time of a $(n+1)$-qubit controlled gate is a little longer than that of a n-qubit controlled gate. Therefore, if this assumption is proved theoretically or experimentally, then it turns out that in our scheme the gate time of a $(n+1)$-qubit controlled gate is much shorter than that of $(2^{n+1}-3)$ or $(10n-9)$ two-qubit controlled gates $(n=3,4,\cdots)$ and the present implementation of $(n+1)$-qubit controlled unitary gates is much more efficient than decomposing into only the elementary gates.

VII. CONCLUSION

In this paper, we have proposed an implementation of multiqubit controlled unitary gates by adiabatic passage with a single-mode optical cavity. A one-qubit $\pi/2$ gate, a two-qubit controlled π gate, and a three-qubit controlled π gate have been numerically simulated. From the simulation results, it has been shown that the present implementation of the three-qubit controlled gates is more efficient than decomposing into the elementary gates. The efficiency of general multiqubit controlled gates is also discussed. If the multiqubit controlled gates can be realized under the condition similar to that for the three-qubit controlled gates, the present implementation of the multiqubit controlled gates will be more efficient than decomposing into the elementary gates. Therefore, if this assumption is proved theoretically or experimentally, then the implementation presented in this paper will be useful to realize quantum algorithms, such as Shor's algorithm for prime factoring or Grover's algorithm for database search.

[1] D. P. DiVincenzo, Phys. Rev. A **51**, 1015 (1995).
[2] A. Barenco *et al.*, Phys. Rev. A **52**, 3457 (1995).
[3] M. A. Nielsen and I. L. Chuang, *Quantum Computation and Quantum Information* (Cambridge University Press, Cambridge, 2000).
[4] S. L. Braunstein *et al.*, *Scalable Quantum Computers* (Wiley-VCH, Berlin, 2001).
[5] P. W. Shor, in *Proceedings of the 35th Annual Symposium on the Foundations of Computer Science*, edited by S. Goldwasser (IEEE Computer Society Press, Los Alamitos, CA, 1994), p. 124.
[6] L. Grover, in *Proceedings of the 28th Annual ACM Symposium on the Theory of Computing* (ACM Press, New York, 1996), p. 212.
[7] V. Vedral, A. Barenco, and A. Ekert, Phys. Rev. A **54**, 147 (1996).
[8] J. I. Cirac and P. Zoller, Phys. Rev. Lett. **74**, 4091 (1995).
[9] M. Šašura and V. Bužek, Phys. Rev. A **64**, 012305 (2001).
[10] M. D. Price *et al.*, Phys. Rev. A **60**, 2777 (1999).
[11] J. Du *et al.*, Phys. Rev. A **63**, 042302 (2001).
[12] V. Giovannetti, D. Vitali, P. Tombesi, and A. Ekert, Phys. Rev. A **62**, 032306 (2000).
[13] B. Qiao, H. E. Ruda, and J. Wang, J. Appl. Phys. **91**, 2524 (2002).
[14] A. O. Niskanen, J. J. Vartiainen, and M. M. Salomaa, Phys. Rev. Lett. **90**, 197901 (2003).
[15] K. Bergmann, H. Theuer, and B. W. Shore, Rev. Mod. Phys. **70**, 1003 (1998).
[16] T. Pellizzari, S. A. Gardiner, J. I. Cirac, and P. Zoller, Phys. Rev. Lett. **75**, 3788 (1995).
[17] Z. Kis and F. Renzoni, Phys. Rev. A **65**, 032318 (2002).
[18] P. Zanardi and M. Rasetti, Phys. Lett. A **264**, 94 (1999).
[19] L.-M. Duan, J. I. Cirac, and P. Zoller, Science **292**, 1695 (2001).
[20] A. Recati *et al.*, Phys. Rev. A **66**, 032309 (2002).
[21] S. J. van Enk, J. I. Cirac, and P. Zoller, Phys. Rev. Lett. **79**, 5178 (1997).
[22] S. Schneider, D. F. V. James, and G. J. Milburn, J. Mod. Opt. **47**, 499 (2000).
[23] J. Pachos and H. Walther, Phys. Rev. Lett. **89**, 187903 (2002).
[24] L. You, X. X. Yi, and X. H. Su, Phys. Rev. A **67**, 032308 (2003).
[25] K. Ichimura, Opt. Commun. **196**, 119 (2001).
[26] M. S. Shahriar *et al.*, Phys. Rev. A **66**, 032301 (2002).
[27] E. Arimondo, in *Progress in Optics*, edited by E. Wolf (Elsevier, Amsterdam, 1996), Vol. 35, p. 257.
[28] M. V. Berry, Proc. R. Soc. London, Ser. A **392**, 45 (1984).
[29] M. Nakahara, *Geometry, Topology and Physics* (IOP, Bristol, 1990).
[30] *Cavity Quantum Electrodynamics*, edited by P. R. Berman, Adv. At. Mol. Opt. Phys. Suppl. 2 (Academic Press, San Diego, 1994).